CAMBRIDGE
UNIVERSITY PRESS

Article

Pseudomeisserite-(NH$_4$), a new mineral with a novel uranyl-sulfate linkage from the Blue Lizard mine, San Juan County, Utah, USA

Anthony R. Kampf[1]* [ID], Travis A. Olds[2], Jakub Plášil[3], Barbara P. Nash[4] and Joe Marty[5]

[1]Mineral Sciences Department, Natural History Museum of Los Angeles County, 900 Exposition Boulevard, Los Angeles, CA 90007, USA; [2]Section of Minerals and Earth Sciences, Carnegie Museum of Natural History, 4400 Forbes Avenue, Pittsburgh, Pennsylvania 15213, USA; [3]Institute of Physics ASCR, v.v.i., Na Slovance 1999/2, 18221 Prague 8, Czech Republic; [4]Department of Geology and Geophysics, University of Utah, Salt Lake City, UT 84112, USA; and [5]5199 East Silver Oak Road, Salt Lake City, UT 84108, USA

Abstract

The new mineral pseudomeisserite-(NH$_4$) (IMA2018-166), (NH$_4$,K)$_2$Na$_4$[(UO$_2$)$_2$(SO$_4$)$_5$]·4H$_2$O, was found in the Blue Lizard mine, San Juan County, Utah, USA, where it occurs as light yellow prisms in a secondary assemblage with belakovskiite, blödite, changoite, ferrinatrite, gypsum, ivsite, metavoltine and tamarugite. The streak is very pale yellow and the fluorescence is bright lime green under 405 nm ultraviolet light. Crystals are transparent with vitreous lustre. The tenacity is brittle, the Mohs hardness is 2½, the fracture is curved or conchoidal and there is one perfect cleavage on {100}. The mineral is easily soluble in H$_2$O and has a measured density of 3.22(2) g·cm^{-3}. Pseudomeisserite-(NH$_4$) is optically biaxial (–) with α = 1.536(2), β = 1.559(2) and γ = 1.565(2) (white light); 2V$_{meas.}$ = 53(1)°; dispersion is r > v, distinct; pleochroism: X colourless, Y light yellow and Z pale yellow (X < Z < Y); optical orientation: Z = **b**, Y ∧ **c** = 33° in obtuse β). Electron microprobe analyses (WDS mode) provided (NH$_4$)$_{1.49}$K$_{0.60}$Na$_{3.87}$U$_{2.00}$S$_{5.04}$O$_{28}$H$_{7.78}$. The five strongest X-ray powder diffraction lines are [d_{obs}, Å(I)(hkl)]: 12.69(76)(100), 6.83(84)(012,102), 6.01(100)($\bar{2}$02), 3.959(67)($\bar{2}$21,$\bar{2}$14,$\bar{1}$23) and 3.135(76)($\bar{2}$06,223,$\bar{1}$16). Pseudomeisserite-(NH$_4$) is monoclinic, P2$_1$/c, a = 13.1010(3), b = 10.0948(2), c = 19.4945(14) Å, β = 104.285(7)°, V = 2498.5(2) Å^3 and Z = 4. The structural unit in the structure (R_1 = 0.0254 for 3837 $I > 2σI$ reflections) is a novel [(UO$_2$)$_2$(SO$_4$)$_5$]$^{6-}$ uranyl-sulfate band.

Introduction

The diverse suite of post-mining uranyl-sulfate minerals found in Red Canyon, Utah, is unlike any other found on Earth. Over the last eight years, 25 new uranyl-sulfate minerals have been described from mines in Red Canyon, mostly from the Blue Lizard mine, but also from the Green Lizard, Markey and Giveaway–Simplot mines. Twenty of these minerals have unique structures among both minerals and synthetic phases and, within their structures, five completely new types of uranyl-sulfate structural units have been identified.

The vast uranyl-sulfate structural diversity is attributable to relatively limited local variations in pH (Plášil *et al.*, 2014), cation abundance and relative humidity, demonstrating that the origins of topological complexity in uranyl-sulfate systems have a highly sensitive crystal-chemical relationship (Gurzhiy and Plášil, 2019). Numerous recent studies of synthetic uranyl-sulfate compounds are supported by our observations of natural structures (Gurzhiy *et al.*, 2016, 2017, 2018, 2019; Lussier *et al.*, 2016; Tyumentseva *et al.*, 2019); however, many arrangements of uranyl and sulfate

polyhedra observed in minerals have yet to be mimicked in the laboratory, including that of pseudomeisserite-(NH$_4$), which includes a previously unreported uranyl-sulfate structural unit. Although the recent sealing of mines in Red Canyon and adjacent areas will limit future discoveries, at least a dozen more Red Canyon uranyl-sulfate phases await characterisation, and the new uranyl-sulfate minerals from Red Canyon continue to be an important source of inspiration for uranyl crystal-chemical and materials-science advances, in general.

Pseudomeisserite-(NH$_4$) is named for its similarity in appearance to meisserite, Na$_5$(UO$_2$)(SO$_4$)$_3$(SO$_3$OH)(H$_2$O) (Plášil *et al.*, 2013). While pseudomeisserite-(NH$_4$) and meisserite do exhibit important chemical and structural differences, in our investigations on the minerals of the Blue Lizard mine, we have found it virtually impossible to distinguish these minerals from one another visually (including under ultraviolet radiation). This is compounded by the fact that they occur in similar associations, and sometimes in close proximity. Note that we prefer 'pseudomeisserite' to 'parameisserite' because the 'para' prefix could be construed as indicating a dimorphous relation. The -(NH$_4$) suffix is used to indicate that this mineral corresponds to the NH$_4$-dominant member of a series that probably exists with a hypothetical K-dominant member. If the latter is described as a mineral, its name should be 'pseudomeisserite-(K)'. Even though the K1 site in the structure exhibits a preference for NH$_4$ and the

K2 site a preference for K, we think that for naming purposes these sites should be considered together.

The new mineral and name were approved by the Commission on New Minerals, Nomenclature and Classification of the International Mineralogical Association (IMA2018-166, Kampf et al., 2019). The description is based on two cotype specimens, both micromounts, deposited in the collections of the Natural History Museum of Los Angeles County, 900 Exposition Boulevard, Los Angeles, CA 90007, USA, catalogue numbers 67621 and 67622.

Occurrence

Pseudomeisserite-(NH$_4$) was found in efflorescent crusts on mine walls underground in the Blue Lizard mine (37°33′26″N, 110° 17′44″W), Red Canyon, White Canyon District, San Juan County, Utah, USA. The mine is ~72 km west of the town of Blanding, Utah, and ~22 km southeast of Good Hope Bay on Lake Powell. The following information on the mine and its geology is taken largely from Chenoweth (1993).

The deposit exploited by the Blue Lizard mine was first recognised in the summer of 1898 by John Wetherill, while leading an archaeological expedition into Red Canyon. He noted yellow stains around a petrified tree. At that spot, he built a rock monument, in which he placed a piece of paper to claim the minerals. Although he never officially recorded his claim, 45 years later, in 1943, he described the spot to Preston V. Redd of Blanding, Utah, who went to the site, found Wetherill's monument and claimed the area as the Blue Lizzard claim (note alternate spelling). Underground workings to mine uranium were not developed until the 1950s.

The uranium deposits in Red Canyon occur within the Shinarump member of the Upper Triassic Chinle Formation, in channels incised into the reddish-brown siltstones of the underlying Lower Triassic Moenkopi Formation. The Shinarump member consists of medium- to coarse-grained sandstone, conglomeratic sandstone beds and thick siltstone lenses. Ore minerals were deposited as replacements of wood and other organic material and as disseminations in the enclosing sandstone. Since the mine closed in 1978, oxidation of primary ores in the humid underground environment has produced a variety of secondary minerals, mainly sulfates, as efflorescent crusts on the surfaces of mine walls.

Pseudomeisserite-(NH$_4$) is a rare mineral in the secondary mineral assemblages of the Blue Lizard mine. It occurs on a thick crust of gypsum overlaying matrix comprised mostly of subhedral to euhedral, equant quartz crystals that are recrystallised counterparts of the original grains of the sandstone. Other secondary phases found in close association with pseudomeisserite-(NH$_4$) are belakovskiite, blödite, changoite, ferrinatrite, ivsite, metavoltine, tamarugite and several other potentially new uranyl sulfates.

Morphology, physical properties and optical properties

Pseudomeisserite-(NH$_4$) crystals are stout prisms, up to ~0.3 mm long, typically occurring in tightly intergrown aggregates (Figs 1 and 2). Prisms are elongate on [010] and exhibit the forms {100}, {001}, {110} and {011} (Fig. 3). No twinning was observed.

The mineral is light yellow with very pale yellow streak and fluoresces bright lime green under 405 nm (long-wave) ultraviolet (UV) laser illumination (for examining micro-crystals, it is often most effective to use lasers, but they are not readily available in
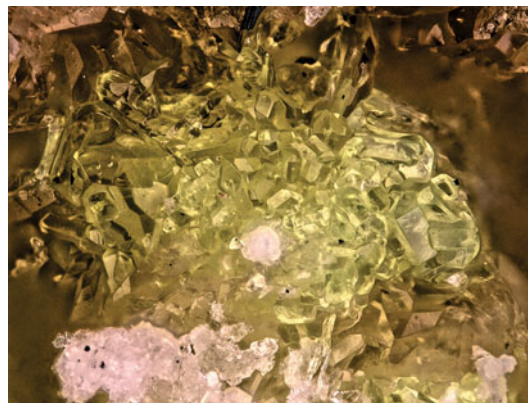

Fig. 1. Intergrown short prisms of pseudomeisserite-(NH$_4$) with white ivsite. The field of view is 0.84 mm across.
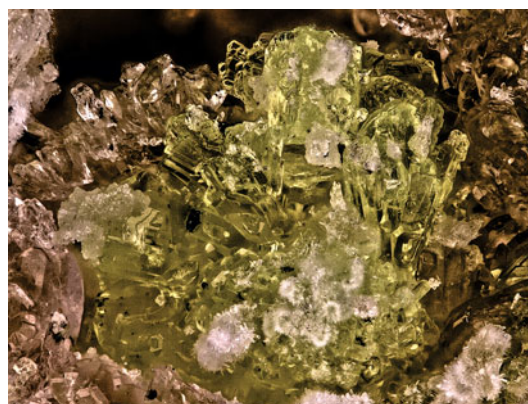
Fig. 2. Intergrown prisms of pseudomeisserite-(NH$_4$) on bladed changoite with white sprays of ferrinatrite. The field of view is 1.0 mm across.
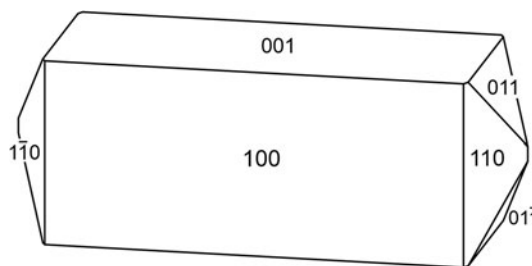
Fig. 3. Crystal drawing of pseudomeisserite-(NH$_4$); clinographic projection in standard orientation.

short-wave; however, uranyl minerals that fluoresce under long-wave UV generally fluoresce similarly under short-wave). Crystals are transparent and have a vitreous lustre. The tenacity is brittle, the Mohs hardness is 2½ (based on scratch tests), the fracture is curved or conchoidal and perfect cleavage on {100} was observed. The density measured by flotation in methylene iodide–toluene is 3.22(2) g·cm^{-3}. The calculated density is 3.277 g·cm^{-3} for the empirical formula and 3.289 g·cm^{-3} for the ideal formula. At room temperature, the mineral is easily soluble in H$_2$O.

Optically, pseudomeisserite-(NH$_4$) is biaxial (–), with α = 1.536(2), β = 1.559(2) and γ = 1.565(2) (measured in white

Fig. 4. The Raman spectrum of pseudomeisserite-(NH₄) recorded with a 785 nm laser.

light). The 2V measured directly on a spindle-stage is 53(1)°; the calculated 2V is 53.5°. Dispersion is $r > v$, distinct. The mineral is pleochroic: X colourless, Y light yellow and Z pale yellow ($X < Z < Y$). The optical orientation is $Z = \mathbf{b}$ and $Y \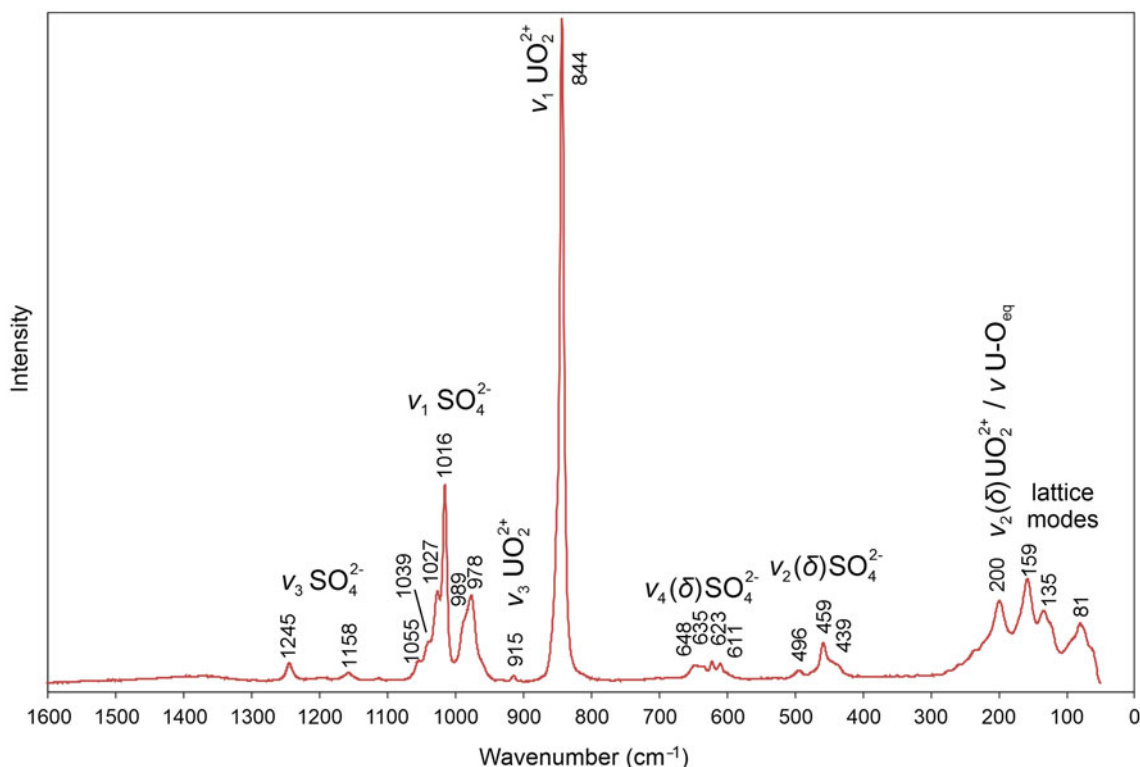wedge \mathbf{c} = 33°$ in obtuse β. The Gladstone-Dale compatibility, $1 - (K_p/K_c)$, is 0.008 (superior) based on the empirical formula (Mandarino, 1981).

Raman spectroscopy

Raman spectroscopy was conducted on a Horiba XploRA PLUS. Pronounced fluorescence was observed using a 532 nm diode laser; consequently, a 785 nm diode laser was utilised. The spectrum, recorded from 1600 to 50 cm⁻¹, is shown in Fig. 4.

The v_3 $(SO_4)^{2-}$ antisymmetric stretching vibrations occur as weak bands at 1245 and 1158 cm⁻¹. Several weak to strong bands/shoulders between 1055 and 978 cm⁻¹ are assignable to the v_1 $(SO_4)^{2-}$ symmetric stretching vibrations. The multiple bands observed in this region are consistent with the presence of several symmetrically unique SO_4 tetrahedra in the pseudomeisserite-(NH₄) structure. The weak band at 915 cm⁻¹ is related to the v_3 $(UO_2)^{2+}$ antisymmetric stretching vibrations. The v_1 $(UO_2)^{2+}$ symmetric stretching vibration is present as a very strong band at 844 cm⁻¹. Bartlett and Cooney (1989) provided an empirical relationship to derive the approximate U–O$_{Ur}$ bond lengths from the band position assigned to the v_1 $(UO_2)^{2+}$ stretching vibration, which gives 1.77 Å, in excellent agreement with U–O$_{Ur}$ bond lengths from the X-ray data: 1.763(4), 1.771(4), 1.765(4) and 1.769(4) Å.

Four weak bands between 648 and 611 cm⁻¹ are attributed to the v_4 (δ) $(SO_4)^{2-}$ bending vibrations, and those at 496, 459 and 439 cm⁻¹ to the v_2 (δ) $(SO_4)^{2-}$ bending vibrations. A band

at 200 cm⁻¹ is attributable to the v_2 (δ) $(UO_2)^{2+}$ bending vibrations and/or possibly to ν U–O$_{eq}$ bending modes. The remaining bands are due to unassigned phonons.

Chemical composition

Chemical analyses (four points on four crystals) were performed at the University of Utah on a Cameca SX-50 electron microprobe with four wavelength dispersive spectrometers and using *Probe for EPMA* software. Analytical conditions were 15 kV accelerating voltage, 10 nA beam current and a beam diameter of 5 μm. Raw X-ray intensities were corrected for matrix effects with a φρ(z) algorithm (Pouchou and Pichoir, 1991). Time-dependent intensity corrections were applied to Na, U and S. Crystals suffered severe beam damage during analyses. Because insufficient material is available for a direct determination of H₂O, it has been calculated based upon the structure determination (U = 2 apfu, O = 28 apfu and charge balance). Analytical data are given in Table 1.

Table 1. Chemical composition of pseudomeisserite-(NH₄).

Constituent	Mean	Range	S.D.	Standard
(NH₄)₂O	3.20	2.98–3.35	0.18	Synthetic Cr₂N
Na₂O	9.90	9.46–10.66	0.55	Albite
K₂O	2.32	2.24–2.44	0.09	Sanidine
UO₃	47.24	46.37–48.15	0.80	Synthetic UO₂
SO₃	33.58	31.80–34.48	1.21	Celestine
H₂O*	5.79			
Total	101.80			

* based on the structure; S.D. – standard deviation.

Table 2. Powder X-ray data (d in Å) for pseudomeisserite-(NH$_4$)*.

I_{obs}	I_{calc}	d_{obs}	d_{calc}	$h\ k\ l$
76	80	**12.69**	12.6959	1 0 0
55	61	**8.88**	8.9034	0 1 1
	10		8.6722	$\bar{1}$ 0 2
12	16	7.94	7.9015	1 1 0
84	30, 62	**6.83**	6.8972, 6.8157	0 1 2, 1 0 2
	5		6.5781	$\bar{1}$ 1 2
100	100	**6.01**	5.9983	$\bar{2}$ 0 2
	13		5.6487	1 1 2
44	49	5.52	5.4787	$\bar{2}$ 1 1
23	30	5.17	5.1566	$\bar{2}$ 1 2
20	10, 7, 12	4.799	4.8764, 4.8334, 4.7536	0 2 1, $\bar{1}$ 0 4, 2 0 2
	8		4.7229	0 0 4
	5		4.6903	1 2 0
51	52	**4.593**	4.5883	$\bar{2}$ 1 3
57	58, 35	**4.414**	4.4581, 4.3595	1 2 1, $\bar{1}$ 1 4
	11		4.3361	$\bar{2}$ 0 4
51	6, 24	4.251	4.3007, 4.2320	2 1 2, 3 0 0
67	19, 11, 5, 57	**3.959**	3.9919, 3.9841, 3.9507, 3.9375	$\bar{2}$ 2 1, $\bar{2}$ 1 4, 2 2 0, $\bar{1}$ 2 3
14	14	3.803	3.8048	1 1 4
20	8, 12, 8	3.667	3.7178, 3.6607, 3.6327	$\bar{3}$ 1 3, 3 1 1, $\bar{1}$ 1 5
12	8, 12	3.556	3.5491, 3.5386	3 0 2, 0 1 5
	9		3.3128	0 3 1
44	41	3.286	3.3020	$\bar{3}$ 2 1
	9		3.2526	1 3 0
41	23, 12, 25	3.230	3.2491, 3.2399, 3.2288	$\bar{1}$ 0 6, $\bar{1}$ 3 1, 2 1 4
	6		3.1721	1 3 1
76	9, 68, 18	**3.135**	3.1467, 3.1368, 3.0928	$\bar{2}$ 0 6, 2 2 3, $\bar{1}$ 1 6
49	8, 22, 8, 19	3.022	3.0278, 3.0247, 3.0173, 3.0058	4 1 0, 0 2 5, 1 3 2, 0 1 6
12	18	2.967	2.9674	$\bar{1}$ 3 3
	5		2.9347	$\bar{2}$ 3 2
17	18	2.892	2.8749	$\bar{4}$ 1 4
29	11, 27	2.815	2.8244, 2.8171	3 0 4, $\bar{2}$ 3 3
	8		2.7817	1 1 6
16	8, 15	2.751	2.7616, 2.7393	$\bar{1}$ 3 4, $\bar{4}$ 2 2
24	6, 13, 9	2.712	2.7199, 2.7042, 2.6922	3 1 4, 4 1 2, $\bar{4}$ 1 5
8	6, 9	2.664	2.6818, 2.6433	$\bar{4}$ 2 3, $\bar{2}$ 1 7
21	21, 14	2.585	2.5859, 2.5760	4 2 1, 2 3 3
11	7	2.502	2.5057	$\bar{5}$ 1 3
11	5, 6, 9, 6	2.453	2.4696, 2.4671, 2.4418, 2.4355	$\bar{1}$ 4 1, $\bar{3}$ 3 4, 1 1 7, $\bar{5}$ 1 4
19	16, 5, 8	2.368	2.3800, 2.3702, 2.3503	0 2 7, 5 1 1, $\bar{2}$ 1 8
	6		2.3430	$\bar{4}$ 3 1
	5		2.3262	$\bar{2}$ 4 2
20	6, 5, 10, 9	2.313	2.3132, 2.3089, 2.3018, 2.2992	5 0 2, 4 3 0, 2 4 1, $\bar{3}$ 2 7
	5		2.2669	1 4 3
10	12	2.219	2.2165	3 1 6
14	14, 10	2.166	2.1675, 2.1493	3 4 0, $\bar{4}$ 3 5
12	5, 5	2.126	2.1242, 2.1107	$\bar{2}$ 3 7, $\bar{1}$ 1 9
12	8, 11, 6	2.045	2.0508, 2.0488, 2.0200	$\bar{5}$ 3 3, $\bar{3}$ 3 7, 3 3 5
	6		2.0153	1 3 7
	11		2.0126	2 1 8
38	6, 6, 7, 5, 13, 9	1.9995	2.0019, 1.9983, 1.9966, 1.9931, 1.9879, 1.9842	4 0 6, 5 2 3, $\bar{4}$ 4 1, $\bar{1}$ 4 6, $\bar{6}$ 2 1, $\bar{2}$ 2 9
15	8, 6	1.9592	1.9637, 1.9539	4 1 6, $\bar{5}$ 1 8
	5		1.9396	$\bar{1}$ 0 10
7	5	1.9254	1.9310	$\bar{4}$ 4 4
7	11	1.8806	1.8819	3 4 4
10	10	1.8502	1.8540	1 2 9
	7		1.8300	2 1 9
32	6, 6, 14, 5, 5	1.8171	1.8191, 1.8175, 1.8137, 1.8119, 1.8072	$\bar{7}$ 1 1, $\bar{5}$ 4 2, 4 1 7, 1 5 4, 4 4 3
13	7, 5, 5	1.7822	1.7907, 1.7861, 1.7746	$\bar{7}$ 1 5, $\bar{6}$ 2 7, 6 0 4
16	7, 6, 5, 6	1.7475	1.7550, 1.7454, 1.7359, 1.7344	3 3 7, $\bar{7}$ 1 6, 1 5 5, $\bar{5}$ 0 10
21	6, 6, 15	1.7045	1.7080, 1.7053, 1.6997	$\bar{3}$ 4 8, 5 4 2, 2 0 10
13	7, 7	1.6616	1.6624, 1.6554	$\bar{1}$ 2 11, 6 1 5
15	5, 8, 5, 6	1.6278	1.6343, 1.6263, 1.6255, 1.6228	$\bar{1}$ 5 7, 2 6 0, $\bar{6}$ 2 9, $\bar{7}$ 2 7
13	6, 5	1.6160	1.6169, 1.6074	4 3 7, $\bar{4}$ 2 11
8	5	1.5664	1.5679	$\bar{7}$ 3 6

* Only calculated lines with $I > 4$ are listed. For $I > 3$ see the supplemental material. The strongest lines are given in bold.

The empirical formula (calculated on the basis of 28 O apfu) is $(NH_4)_{1.49}K_{0.60}Na_{3.87}U_{2.00}S_{5.04}O_{28}H_{7.78}$. The simplified formula is $(NH_4,K)_2Na_4[(UO_2)_2(SO_4)_5]\cdot4H_2O$. The ideal formula is $(NH_4)_2Na_4[(UO_2)_2(SO_4)_5]\cdot4H_2O$, which requires $(NH_4)_2O$ 4.27, Na_2O 10.16, UO_3 46.87, SO_3 32.80 and H_2O 5.90, total 100 wt.%.

X-ray crystallography and structure refinement

Powder X-ray studies were carried out using a Rigaku R-Axis Rapid II curved imaging plate microdiffractometer, with monochromatic $MoK\alpha$ radiation. A Gandolfi-like motion on the φ and ω axes was used to randomise the samples and observed d values and intensities were derived by profile fitting using JADE 2010 software (Materials Data, Inc.). The observed powder data for pseudomeisserite-(NH_4), presented in Table 2, show good agreement with the pattern calculated from the structure refinement. The unit-cell parameters refined from the powder data using JADE 2010 with whole pattern fitting are $a = 13.129(7)$, $b = 10.108(7)$, $c = 19.534(7)$ Å, $\beta = 104.315(12)°$ and $V = 2512(2)$ Å³.

Single-crystal X-ray studies were done using the same diffractometer and radiation used for the powder studies. The Rigaku CrystalClear software package was used for processing the structure data, including the application of an empirical absorption correction using the multi-scan method with ABSCOR (Higashi, 2001). The structure was solved by the charge-flipping method using SHELXT (Sheldrick, 2015a). SHELXL-2016 (Sheldrick, 2015b) was used for the refinement of the structure. Two large-cation sites were refined with full joint occupancies by K and N (NH_4). The N1 site refined to $N_{0.386}K_{0.614(9)}$, while the N2 site refined to $N_{0.767}K_{0.233(10)}$. A difference-Fourier syntheses located all H atom positions associated with the H_2O groups, which were then refined with soft restraints of 0.82(3) Å on the O–H distances and 1.30(3) Å on the H–H distances and with the U_{eq} of each H set to 1.2 times that of the donor O atom. However, the H atom positions associated with the NH_4 cations were not resolved at this stage of the refinement.

The equivalent isotropic displacement parameters (U_{eq}) of the N1 and N2 sites refined to 0.042 and 0.056, respectively, significantly greater than those of the Na sites (0.021 to 0.037). The total of the refined joint occupancies of the N1 and N2 sites provided a large-cation content of $[(NH_4)_{1.15}K_{0.85}]_{\Sigma2.00}$, compared with the much more NH_4-rich content of $[(NH_4)_{1.49}K_{0.60}]_{\Sigma2.09}$ obtained from the electron-probe microanalyses (EPMA). These factors suggested that the N1 and N2 sites actually have more N and less K than the refinement indicated. To explore this, we adjusted the occupancies to $N_{0.50}K_{0.50}$ and $N_{0.91}K_{0.09}$, respectively, so that these sites refined to U_{eq} values of ~0.031 and provided a total content of $[(NH_4)_{1.41}K_{0.59}]_{\Sigma2.00}$. The R_1 increased from 0.0251 to 0.0259; however, potential H positions associated with the N sites were revealed. When these were incorporated into the refinement, R_1 decreased to 0.0253. In the final refinement, with H positions included, the joint N/K occupancies of the N1 and N2 sites were again refined, yielding N1: $N_{0.446}K_{0.554(10)}$ and N2: $N_{0.880}K_{0.120(11)}$, with a final total large-cation content of $[(NH_4)_{1.33}K_{0.67}]_{\Sigma2}$, a final R_1 of 0.0252 and U_{eq} values of 0.037 for the N sites. The H sites associated with the N1 and N2 sites were refined with soft restraints of 0.90(3) Å on the N–H distances and 1.45(3) Å on the H–H distances and with the U_{eq} of each H set to 1.5 times that of the donor N atom; the occupancies of the H sites were tied to those of the corresponding N sites.

Table 3. Data collection and structure refinement details for pseudomeisserite-(NH_4).

Crystal data	
Structural formula	$[(NH_4)_{1.33}K_{0.67}]_{\Sigma2}Na_4[(UO_2)_2(SO_4)_5]\cdot4H_2O$
Crystal size (µm)	70 × 50 × 50
Crystal system, space group	Monoclinic, $P2_1/c$
Temperature (K)	293(2)
Unit-cell dimensions	
a, b, c (Å)	13.1010(3), 10.0948(2), 19.4945(14)
β (°)	104.285(7)
V (Å³)	2498.5(2)
Z	4
Density (for above formula) (g cm⁻³)	3.282
µ (mm⁻¹)	13.669
$F(000)$	2269.6
Data collection	
Diffractometer	Rigaku R-Axis Rapid II
X-ray radiation/power	$MoK\alpha$ ($\lambda = 0.71075$ Å)/50 kV, 40 mA
θ range (°)	3.10 to 25.03
Absorption correction	Multi-scan, Higashi (2001)
T_{min}, T_{max}	0.752, 1.000
Refl. collected/unique	17556, 4394
Reflections with $I > 2\sigma I$	3838
R_{int}	0.046
Completeness to θ = 25.03°	99.6%
Index ranges	$-15 \leq h \leq 15$, $-12 \leq k \leq 10$, $-23 \leq l \leq 23$
Refinement	
Refinement method	Full-matrix least-squares on F^2
Parameters/restraints	420/32
GoF	1.075
Final R indices [$I > 3\sigma I$]	$R_1 = 0.0252$, $wR_2 = 0.0455$
R indices (all data)	$R_1 = 0.0323$, $wR_2 = 0.0475$
$\Delta\rho_{max}$, $\Delta\rho_{min}$ (e^-Å⁻³)	+1.167/−0.97

$R_{int} = \Sigma|F_o^2-F_o^2(mean)|/\Sigma[F_o^2]$. GoF = $S = \{\Sigma[w(F_o^2-F_c^2)^2]/(n-p)\}^{1/2}$. $R_1 = \Sigma||F_o|-|F_c||/\Sigma|F_o|$. $wR_2 = \{\Sigma[w(F_o^2-F_c^2)^2]/\Sigma[w(F_o^2)^2]\}^{1/2}$; $w = 1/[\sigma^2(F_o^2)+(aP)^2+bP]$ where a is 0.0115, b is 8.0215 and P is $[2F_c^2+Max(F_o^2,0)]/3$.

Data collection and refinement details are given in Table 3, atom coordinates and displacement parameters in Table 4, selected bond distances in Table 5 and bond-valence summations (BVS) in Table 6. The crystallographic information files have been deposited with the Principal Editor of Mineralogical Magazine and are available as Supplementary material (see below).

Description of the structure

The U1 and U2 sites in the structure of pseudomeisserite-(NH_4) are each surrounded by seven O atom sites forming pentagonal bipyramids. This is a most frequent coordination for U^{6+} in mineral and inorganic structures where the two short apical bonds of the bipyramid constitute the uranyl group (cf. Burns, 2005). The two apical O atoms of the bipyramids (O_{Ur}) form short bonds with the U, and this unit comprises the UO_2^{2+} uranyl group. Five equatorial O atoms (O_{eq}) complete each of the U coordinations. All O_{eq} atoms bound to U also participate in SO_4 groups. The U1 bipyramid is surrounded by five SO_4 groups [centred by S1 (×2), S2 and S5 (×2)], each of which shares one O_{eq} corner of the U1 bipyramid. The U2 bipyramid is surrounded by four SO_4 groups, three of which (centred by S1, S2 and S3) share single O_{eq} corners and one of which (centred by S4) shares two equatorial O atoms, a polyhedral edge. Such a bidentate linkage between a UO_7 pentagonal bipyramid and a SO_4 tetrahedron has been previously reported in the Na-uranyl-sulfate minerals klaprothite, péligotite and ottohahnite (Kampf et al., 2017b) and lussierite

Table 4. Atom coordinates and displacement parameters (Å^2) for pseudomeisserite-(NH$_4$).

	x/a	y/b	z/c	U$_{eq}$	U^{11}	U^{33}	U^{23}	U^{13}	U^{12}	U^{22}
N1*	0.0613(2)	0.7857(2)	0.45287(12)	0.0369(11)	0.046(2)	0.0383(17)	0.0288(16)	0.0001(10)	0.0138(12)	0.0041(12)
HN1A	0.121(5)	0.771(12)	0.485(5)	0.055						
HN1B	0.007(6)	0.771(11)	0.472(6)	0.055						
HN1C	0.056(9)	0.726(9)	0.418(4)	0.055						
HN1D	0.059(9)	0.866(5)	0.435(6)	0.055						
N2*	0.1370(2)	0.3683(4)	0.1685(2)	0.037(2)	0.035(4)	0.039(3)	0.037(3)	0.001(2)	0.005(2)	−0.004(2)
HN2A	0.111(5)	0.433(5)	0.193(3)	0.056						
HN2B	0.189(4)	0.404(6)	0.153(3)	0.056						
HN2C	0.087(4)	0.336(6)	0.136(3)	0.056						
HN2D	0.163(5)	0.308(5)	0.203(3)	0.056						
Na1	0.55001(19)	0.6688(2)	0.99930(12)	0.0212(5)	0.0211(14)	0.0217(13)	0.0204(13)	0.0026(10)	0.0043(11)	0.0002(11)
Na2	0.2169(2)	0.7155(2)	0.15605(13)	0.0262(6)	0.0237(15)	0.0324(15)	0.0217(14)	0.0011(11)	0.0043(12)	−0.0021(12)
Na3	0.1340(2)	0.9479(3)	0.28039(14)	0.0367(7)	0.0337(18)	0.0424(17)	0.0351(17)	−0.0018(13)	0.0109(14)	0.0062(14)
Na4	0.3572(2)	0.6849(3)	0.35164(14)	0.0299(6)	0.0232(16)	0.0371(16)	0.0273(15)	−0.0065(11)	0.0022(12)	0.0005(12)
U1	0.50946(2)	0.65871(2)	0.70504(2)	0.01159(6)	0.01304(13)	0.01045(12)	0.01107(12)	0.00012(8)	0.00255(9)	−0.00008(9)
U2	0.20097(2)	0.39493(2)	0.46067(2)	0.01369(7)	0.01267(13)	0.01414(13)	0.01318(12)	0.00018(8)	0.00114(9)	−0.00074(9)
S1	0.62563(11)	0.65210(13)	0.36472(7)	0.0123(3)	0.0137(8)	0.0111(7)	0.0109(7)	−0.0003(5)	0.0010(6)	−0.0010(6)
S2	0.34771(12)	0.68412(14)	0.52439(7)	0.0150(3)	0.0188(9)	0.0149(8)	0.0117(7)	−0.0006(6)	0.0048(6)	−0.0040(6)
S3	0.11756(13)	0.60632(15)	0.30045(8)	0.0199(3)	0.0193(9)	0.0222(9)	0.0164(8)	0.0008(6)	0.0011(7)	0.0022(7)
S4	0.94659(12)	0.65482(15)	0.08826(8)	0.0187(3)	0.0151(9)	0.0190(8)	0.0200(8)	0.0027(6)	0.0002(7)	0.0029(7)
S5	0.42770(12)	0.48767(13)	0.84582(7)	0.0125(3)	0.0167(8)	0.0096(7)	0.0121(8)	0.0005(5)	0.0051(6)	−0.0001(6)
O1	0.5406(3)	0.6849(4)	0.3973(2)	0.0220(10)	0.022(3)	0.022(2)	0.025(2)	0.0001(18)	0.010(2)	0.0055(19)
O2	0.6299(3)	0.7455(4)	0.30741(19)	0.0147(9)	0.018(2)	0.012(2)	0.011(2)	0.0056(15)	−0.0009(18)	0.0014(17)
O3	0.6137(3)	0.5162(4)	0.3352(2)	0.0182(9)	0.021(3)	0.014(2)	0.020(2)	−0.0030(16)	0.0067(19)	−0.0017(18)
O4	0.7295(3)	0.6588(4)	0.4168(2)	0.0205(10)	0.020(2)	0.024(2)	0.015(2)	0.0043(17)	0.0005(19)	−0.0060(19)
O5	0.2571(3)	0.7225(4)	0.5505(2)	0.0269(11)	0.022(3)	0.029(3)	0.034(3)	−0.001(2)	0.014(2)	−0.001(2)
O6	0.3620(3)	0.7699(4)	0.4669(2)	0.0198(10)	0.026(3)	0.017(2)	0.017(2)	0.0050(17)	0.008(2)	0.0004(19)
O7	0.3352(3)	0.5458(4)	0.4973(2)	0.0184(9)	0.019(2)	0.011(2)	0.024(2)	−0.0020(17)	0.0022(19)	−0.0039(18)
O8	0.4472(3)	0.6895(4)	0.5815(2)	0.0229(10)	0.024(3)	0.026(2)	0.016(2)	−0.0026(17)	0.000(2)	−0.012(2)
O9	0.0557(5)	0.7038(6)	0.3260(3)	0.071(2)	0.053(4)	0.085(5)	0.060(4)	−0.036(3)	−0.014(3)	0.045(4)
O10	0.1931(4)	0.6732(5)	0.2687(3)	0.0478(15)	0.043(4)	0.068(4)	0.027(3)	0.017(2)	0.000(3)	−0.033(3)
O11	0.0512(3)	0.5159(4)	0.2499(2)	0.0270(11)	0.022(3)	0.035(3)	0.021(2)	−0.0012(19)	−0.001(2)	−0.007(2)
O12	0.1808(4)	0.5286(4)	0.3609(2)	0.0314(11)	0.032(3)	0.033(3)	0.024(3)	0.013(2)	−0.003(2)	−0.003(2)
O13	0.0566(3)	0.6338(4)	0.0923(2)	0.0257(10)	0.017(3)	0.027(3)	0.033(3)	0.0037(19)	0.008(2)	0.008(2)
O14	0.8948(3)	0.5376(4)	0.1076(2)	0.0271(11)	0.022(3)	0.030(3)	0.026(3)	0.0026(19)	−0.001(2)	−0.005(2)
O15	0.9293(3)	0.7717(4)	0.1315(2)	0.0220(10)	0.021(3)	0.026(2)	0.019(2)	−0.0005(18)	0.002(2)	0.006(2)
O16	0.8905(3)	0.6960(4)	0.0142(2)	0.0201(10)	0.024(3)	0.019(2)	0.016(2)	0.0008(17)	0.0023(19)	0.0081(19)
O17	0.4794(3)	0.4959(4)	0.9202(2)	0.0185(9)	0.022(3)	0.018(2)	0.014(2)	−0.0034(16)	0.0026(19)	−0.0024(18)
O18	0.3329(3)	0.5676(4)	0.8256(2)	0.0202(9)	0.018(2)	0.017(2)	0.026(2)	−0.0003(18)	0.008(2)	0.0054(19)
O19	0.4008(3)	0.3458(4)	0.8275(2)	0.0148(9)	0.017(2)	0.012(2)	0.016(2)	−0.0020(16)	0.0043(18)	−0.0014(17)
O20	0.5048(3)	0.5304(4)	0.8043(2)	0.0157(9)	0.020(2)	0.009(2)	0.020(2)	0.0034(16)	0.0075(19)	−0.0036(17)
O21	0.6130(3)	0.5567(4)	0.6930(2)	0.0192(9)	0.022(3)	0.014(2)	0.024(2)	−0.0017(17)	0.008(2)	0.0009(18)
O22	0.4054(3)	0.7582(4)	0.7199(2)	0.0183(9)	0.021(2)	0.014(2)	0.021(2)	0.0007(17)	0.0061(19)	0.0037(18)
O23	0.1037(3)	0.4923(4)	0.4857(2)	0.0271(11)	0.019(3)	0.027(3)	0.036(3)	0.000(2)	0.009(2)	0.004(2)
O24	0.2969(3)	0.2955(4)	0.4359(2)	0.0191(10)	0.020(3)	0.015(2)	0.022(2)	−0.0010(17)	0.0049(19)	0.0004(18)
OW1	0.1454(5)	0.9315(5)	0.1609(3)	0.0463(14)	0.058(4)	0.040(3)	0.041(4)	−0.001(2)	0.013(3)	0.004(3)
H1A	0.105(4)	0.969(7)	0.128(3)	0.056						
H1B	0.204(3)	0.960(8)	0.161(4)	0.056						
OW2	0.1825(4)	0.1893(5)	0.2654(2)	0.0281(11)	0.018(3)	0.038(3)	0.031(3)	0.003(2)	0.011(2)	0.000(2)
H2A	0.243(2)	0.193(7)	0.287(3)	0.034						
H2B	0.148(4)	0.219(6)	0.291(3)	0.034						
OW3	0.2737(4)	0.4991(4)	0.1282(2)	0.0269(11)	0.030(3)	0.026(3)	0.025(3)	0.010(2)	0.007(2)	0.010(2)
H3A	0.268(5)	0.494(6)	0.0859(14)	0.032						
H3B	0.331(3)	0.470(6)	0.148(3)	0.032						
OW4	0.7012(4)	0.5243(4)	0.0028(2)	0.0245(10)	0.024(3)	0.021(3)	0.025(3)	−0.0021(19)	0.001(2)	−0.006(2)
H4A	0.750(4)	0.540(6)	0.035(2)	0.029						
H4B	0.676(4)	0.457(4)	0.012(3)	0.029						

* Refined occupancies: N1: N$_{0.446}$K$_{0.554(10)}$ and N2: N$_{0.880}$K$_{0.120(11)}$

(Kampf *et al.*, 2019; Fig. 5*a*), all of which occur at the Blue Lizard mine.

The U1 bipyramids are linked to one another by pairs of SO$_4$ tetrahedra (centred by S1 and S5) to form a chain along **b**. This chain is topologically identical to those in meisserite (Plášil *et al.*, 2013; Fig. 5*b*) and fermiite (Kampf *et al.*, 2015), both of which occur at the Blue Lizard mine. However, in the structure of pseudomeisserite-(NH$_4$), each U1 bipyramid in the chain is

also linked to a U2 bipyramid by pairs of SO$_4$ tetrahedra (centred by S1 and S2), thereby yielding a $[(UO_2)_2(SO_4)_5]^{6-}$ uranyl-sulfate band (Fig. 5*c*) having its plane parallel to {10$\bar{1}$}. This band is the structural unit in the structure of pseudomeisserite-(NH$_4$). To our knowledge, no similar structural unit has been previously reported in the structure of any mineral or synthetic compound. The complexity of U–S polyhedral linkage contributes apparently to the overall complexity of the pseudomeisserite-(NH$_4$) structure.

Table 5. Selected bond distances (Å) for pseudomeisserite-(NH₄).*

Na1–O17	2.361(4)	Na3–O11	2.449(5)	U1–O21	1.764(4)	S1–O1	1.451(4)	S4–O13	1.440(4)	N1–O9*	2.592(6)
Na1–O17	2.381(4)	Na3–O14	2.477(5)	U1–O22	1.774(4)	S1–O2	1.474(4)	S4–O14	1.459(4)	N1–O16*	2.791(5)
Na1–OW4	2.448(5)	Na3–O18	2.542(5)	U1–O20	2.342(4)	S1–O3	1.481(4)	S4–O15	1.499(4)	N1–O13	2.853(5)
Na1–O24	2.450(5)	Na3–OW2	2.554(6)	U1–O8	2.365(4)	S1–O4	1.485(4)	S4–O16	1.508(4)	N1–O5*	2.864(5)
Na1–O1	2.455(5)	Na3–O9	2.892(8)	U1–O3	2.390(4)	<S1–O>	1.473	<S4–O>	1.477	N1–O14*	2.919(5)
Na1–O6	2.466(5)	Na3–O10	2.903(6)	U1–O19	2.392(4)					N1–O23	3.052(5)
Na1–O8	2.737(5)	<Na3–O>	2.599	U1–O23	2.419(4)	S2–O5	1.454(4)	S5–O17	1.444(4)	<N1–O>	2.845
<Na1–O>	2.471			<U1–O_Ur>	1.769	S2–O6	1.465(4)	S5–O18	1.451(4)		
		Na4–O1	2.347(5)	<U1–O_eq>	2.382	S2–O7	1.487(4)	S5–O19	1.497(4)	N2–OW3*	2.502(6)
Na2–O13	2.313(5)	Na4–O10	2.352(6)			S2–O8	1.492(4)	S5–O20	1.505(4)	N2–OW2*	2.575(7)
Na2–O5	2.332(5)	Na4–O6	2.391(5)	U2–O24	1.766(4)	<S2–O>	1.475	<S5–O>	1.474	N2–O11*	2.623(6)
Na2–O10	2.332(5)	Na4–O18	2.554(5)	U2–O23	1.770(4)					N2–O9	3.046(7)
Na2–OW1	2.384(6)	Na4–O21	2.650(4)	U2–O7	2.302(4)	S3–O9	1.439(5)			N2–O13	3.118(6)
Na2–OW3	2.413(5)	Na4–O12	2.840(5)	U2–O12	2.328(4)	S3–O10	1.457(5)			N2–O2	3.221(6)
Na2–O22	2.490(5)	Na4–O22	2.850(5)	U2–O41	2.399(4)	S3–O11	1.463(4)			<N2–O>	2.848
<Na2–O>	2.377	<Na4–O>	2.569	U2–O16	2.450(4)	S3–O12	1.486(4)				
				U2–O15	2.485(4)	<S3–O>	1.461				
				U2–O_Ur>	1.768						
				U2–O_eq>	2.393						

Hydrogen bonds

D–H···A	D–H	H···A	D···A	<DHA
N1–HN1A···O5*	0.89(3)	1.98(3)	2.864(5)	174(11)
N1–HN1B···O16*	0.89(3)	1.93(5)	2.791(5)	161(11)
N1–HN1C···O9*	0.91(3)	1.80(6)	2.592(6)	145(10)
N1–HN1D···O14*	0.88(3)	2.08(5)	2.919(5)	160(11)
N2–HN1A···O11*	0.91(3)	1.73(3)	2.623(6)	164(6)
N2–HN1B···OW3*	0.88(2)	1.63(3)	2.502(6)	168(7)
N2–HN1D···OW2*	0.91(3)	1.69(3)	2.575(7)	166(6)
OW1–H1A···O23	0.81(3)	2.80(6)	3.413(7)	133(7)
OW1–H1B···O3	0.82(3)	2.44(3)	3.252(7)	172(8)
OW2–H2A···O19	0.81(3)	2.06(3)	2.840(6)	164(6)
OW2–H2B···O15	0.80(3)	2.09(3)	2.887(6)	170(7)
OW3–H3A···OW4	0.81(3)	1.88(3)	2.664(6)	162(6)
OW3–H3B···O20	0.81(3)	2.12(4)	2.891(6)	158(7)
OW4–H4A···O14	0.80(3)	2.06(3)	2.840(6)	164(7)
OW4–H4B···O6	0.80(3)	2.02(3)	2.806(6)	169(7)

* Ordered N–H···O hydrogen bonds.

Table 6. Bond valence analysis for pseudomeisserite-(NH₄). Values are expressed in valence units.*

	N1	N2	Na1	Na2	Na3	Na4	U1	U2	S1	S2	S3	S4	S5	Hydrogen bonds	Sum
O1			0.17			0.21			1.58						1.96
O2		0.06							1.49						2.00
O3							0.48		1.47					0.10	2.05
O4								0.47	1.45						1.92
O5	0.15			0.22						1.57					1.94
O6			0.16			0.19				1.53				0.18	2.06
O7								0.58		1.45					2.03
O8			0.08				0.51			1.43					2.02
O9	0.30	0.10			0.06						1.63				2.09
O10				0.22	0.06	0.21					1.56				2.05
O11		0.32			0.17						1.54				2.03
O12							0.07	0.55			1.45				2.07
O13	0.15	0.09		0.23								1.61			2.08
O14	0.13				0.16							1.55		0.17	2.01
O15								0.40				1.40		0.16	1.96
O16	0.18							0.43				1.37			1.98
O17			0.20										1.61		2.01
			0.20												
O18					0.13	0.13							1.58		1.84
O19							0.48						1.41	0.17	2.06
O20							0.53						1.38	0.16	2.07
O21						0.10	1.82								1.92
O22				0.15		0.06	1.78								1.99
O23	0.09							1.79						0.08	1.96
O24			0.17					1.81							1.98
OW1				0.19	0.20									−0.08, −0.10	0.21
OW2		0.37			0.13									−0.16, −0.17	0.17
OW3		0.45		0.18										−0.24, −0.16	0.23
OW4			0.16											0.24, −0.18, −0.17	0.06
Sum	1.00	1.39	1.14	1.19	0.91	0.97	6.05	6.03	5.99	5.98	6.18	5.93	5.98		

*The N1 and N2 site bond valences are based on refined joint occupancies by K and N. NH₄⁺–O bond valence parameters are from García-Rodríguez *et al.* (2000). All other cation–O bond valence parameters are from Gagné and Hawthorne (2015). Hydrogen-bond strengths are based on O–O bond lengths from Ferraris and Ivaldi (1988).
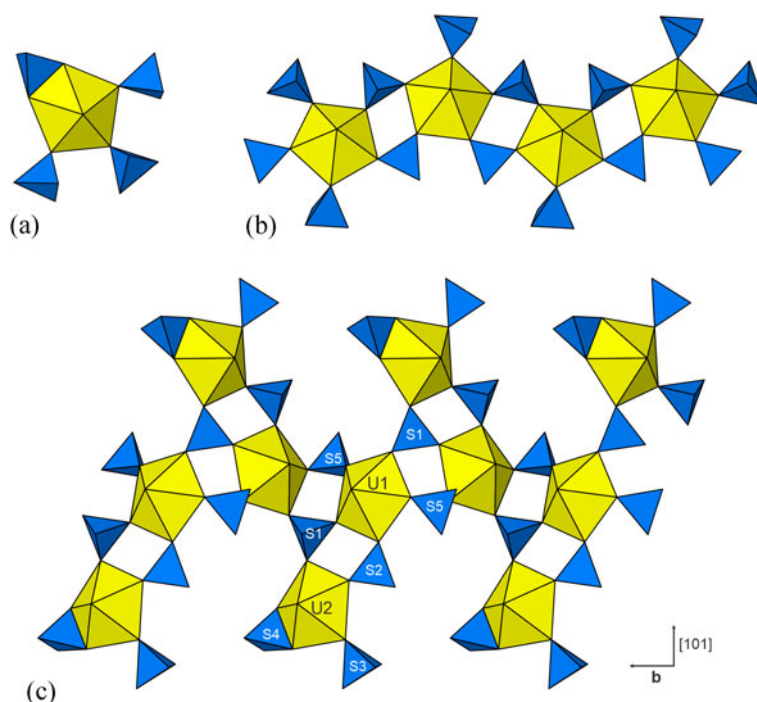
Fig. 5. (*a*) The $[(UO_2)(SO_4)_4]^{6-}$ cluster in lussierite. (*b*) The $[(UO_2)(SO_4)_3]^{4-}$ chain in meisserite. (*c*) The $[(UO_2)_2(SO_4)_5]^{6-}$ band in pseudomeisserite-(NH₄).
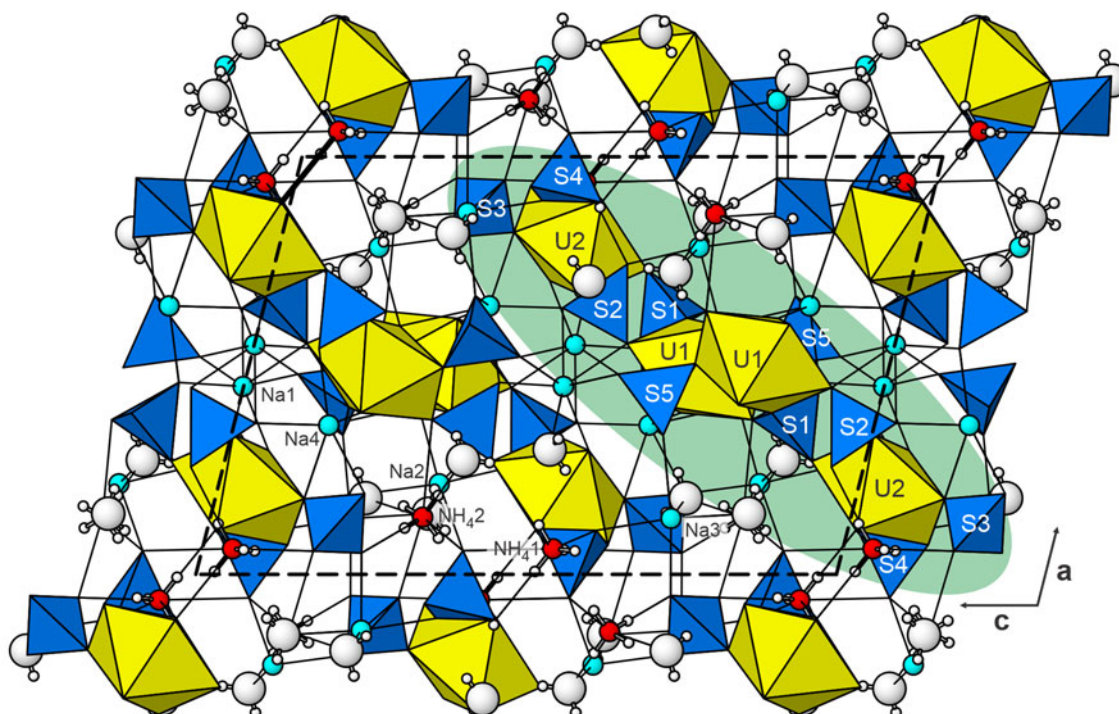

Fig. 6. The crystal structure of pseudomeisserite-(NH₄) viewed down **b**. The Na–O and NH₄/K–O bonds are shown as thin black lines. Hydrogen bonds are not shown. The $[(UO_2)_2(SO_4)_5]^{6-}$ band is highlighted with a green background. The unit cell is indicated by dashed lines.

With total complexity of 1329.90 bits/cell (including hydrogen atoms), pseudomeisserite-(NH₄) is one of the very complex uranyl minerals (after Krivovichev, 2013) and belongs to group of most complex uranyl sulfates (Gurzhiy and Plášil, 2019). Based on the topological type of structural unit, it falls in the group of structures that are based on dense chains of polyhedra, such as alwilkinsite-(Y) (Kampf *et al.*, 2017a) and uranopilite (Burns, 2001).

The uranyl sulfate bands are linked through a complex network of bonds involving two large-cation sites (N1 and N2) occupied jointly by NH₄ and K, four Na sites (Na1, Na2, Na3 and Na4) and four H₂O-group sites (OW1, OW2, OW3 and OW4). The K1, K2 and Na2 sites are six coordinated, while the Na1, Na3 and Na4 sites are seven coordinated. The entire structure is shown in Fig. 6, with one uranyl-sulfate band highlighted.

The N1 site appears to accommodate roughly equivalent amounts of NH_4 and K, while the N2 site exhibits a significantly greater affinity for NH_4 over K. There is no obvious explanation for the preference of the N2 site for NH_4; in fact, NH_4 prominence in the N2 site is counter-indicated by bond-valence considerations (considering NH_4 as a spherical cation), as the high BVS for the site (1.39 valence units) would be close to neutral (1.02 vu) with occupancy by K alone. It is worth noting that the bond-valence values reported in Table 6 follow the approach of Garcia-Rodriguez *et al.* (2000), which treats NH_4^+ strictly as a spherical cation. Other authors (*cf.* Khan and Baur, 1972) have studied ordered hydrogen bonding exhibited in some NH_4 coordinations. Catti and Franchini-Angela (1976) noted that, for short $H{\cdots}O$ bonds with large $N–H{\cdots}O$ angles, the NH_4^+ group behaves as an ordered hydrogen-bond donor, while long $H{\cdots}O$ distances and relatively small $N–H{\cdots}O$ angles are indicative of behaviour as a strongly electropositive large alkali-like cation. It seems reasonable to assume that $NH_4–O$ bonds corresponding to ordered hydrogen bonds provide somewhat greater bond strength than those corresponding to electrostatic bonds, and that this should be particularly true for relatively short $N–H{\cdots}O$ bonds. The N1 and N2 coordinations in the structure of pseudomeisserite each include ordered hydrogen bonds (see Table 6). The N1 site has four such bonds and the N2 site has three. That suggests that the N1 site might be more favourable to NH_4 over K; however, the fact that the three ordered $N–H{\cdots}O$ bonds for the N2 site are particularly short may make this site more favourable for NH_4 occupancy.

References

Bartlett J.R. and Cooney R.P. (1989) Short communication SPECTROSCOPY. *Science and Technology*, **193**, 295–300.

Burns P.C. (2001) A new uranyl sulfate chain in the structure of uranopilite. *The Canadian Mineralogist*, **39**, 1139–1146.

Burns P.C. (2005) U^{6+} minerals and inorganic compounds: Insights into an expanded structural hierarchy of crystal structures. *The Canadian Mineralogist*, **43**, 1839–1894.

Catti M. and Franchini-Angela M. (1976) Hydrogen bonding in the crystalline state. Structure of $Mg_3(NH_4)_2(HPO_4)_4.8H_2O$ (hannayite), and crystal-chemical relationships with schertelite and struvite. *Acta Crystallographica*, **B32**, 2842–2848.

Chenoweth W.L. (1993) *The Geology and Production History of the Uranium Deposits in the White Canyon Mining District, San Juan County, Utah*. Utah Geological Survey Miscellaneous Publication, 93–3.

Ferraris G. and Ivaldi G. (1988) Bond valence vs bond length in $O{\cdots}O$ hydrogen bonds. *Acta Crystallographica*, **B44**, 341–344.

Gagné O.C. and Hawthorne F.C. (2015) Comprehensive derivation of bond-valence parameters for ion pairs involving oxygen. *Acta Crystallographica*, **B71**, 562–578.

García-Rodríguez L., Rute-Pérez Á., Piñero J.R. and González-Silgo C. (2000) Bond-valence parameters for ammonium-anion interactions. *Acta Crystallographica*, **B56**, 565–569.

Gurzhiy V.V. and Plášil J. (2019) Structural complexity of natural uranyl sulfates. *Acta Crystallographica*, **B75**, 39–48.

Gurzhiy V.V., Tyumentseva O.S., Krivovichev S.V., Krivovichev V.G. and Tananaev I.G. (2016) Mixed uranyl sulfate–selenates: Evolution of structural topology and complexity vs chemical composition. *Crystal Growth & Design*, **16**, 4482–4492.

Gurzhiy V.V., Tyumentseva O.S., Krivovichev S.V. and Tananaev I.G. (2017) Selective Se-for-S substitution in Cs-bearing uranyl compounds. *Journal of Solid State Chemistry*, **248**, 126–133.

Gurzhiy V.V., Tyumentseva O.S., Krivovichev S.V. and Tananaev I.G. (2018) Cyclic polyamines as templates for novel complex topologies in uranyl sulfates and selenates. *Zeitschrift für Kristallographie – Crystalline Materials*, **233**, 233–245.

Gurzhiy V.V., Tyumentseva O.S., Izatulina A.R., Krivovichev S.V. and Tananaev I.G. (2019) Chemically induced polytypic phase transitions in the $Mg[(UO_2)(TO_4)_2(H_2O)](H_2O)_4$ (T = S, Se) system. *Inorganic Chemistry*, **58**, 14760–14768.

Higashi T. (2001) *ABSCOR*. Rigaku Corporation, Tokyo.

Kampf A.R., Plášil J., Kasatkin A. V., Marty J. and Čejka J. (2015) Fermiite, $Na_4(UO_2)(SO_4)_3{\cdot}3H_2O$, and oppenheimerite, $Na_2(UO_2)(SO_4)_2{\cdot}3H_2O$. *Mineralogical Magazine*, **79**, 1123–1142.

Kampf A.R., Plášil J., Čejka J., Marty J., Škoda R. and Lapčák L. (2017a) Alwilkinsite-(Y), a new rare-earth uranyl sulfate mineral from the Blue Lizard mine, San Juan County, Utah, USA. *Mineralogical Magazine*, **81**, 895–907.

Kampf A.R., Plášil J., Kasatkin A.V., Marty J. and Čejka J. (2017b) Klaprothite, péligotite and ottohahnite, three new minerals with bidentate $UO_7–SO_4$ linkages from the Blue Lizard mine, San Juan County, Utah, USA. *Mineralogical Magazine*, **81**, 753–779.

Kampf A.R., Olds T.A., Plášil J., Nash B.P. and Marty J. (2019) Pseudomeisserite-(NH4), IMA 2018-166. CNMNC Newsletter No. 49, June 2019, page 482; *Mineralogical Magazine*, **83**, 323–328.

Kampf A.R., Olds T.A., Plášil J., Nash B.P. and Marty J. (2019) Lussierite, a new sodium-uranyl-sulfate mineral with bidentate $UO_7–SO_4$ linkage from the Blue Lizard mine, San Juan County, Utah, USA. *Mineralogical Magazine*, **83**, 799–808

Khan A.A. and Baur W.H. (1972) Salt hydrates. VIII. The crystal structures of sodium ammonium orthochromate dihydrate and magnesium diammonium bis(hydrogen orthophosphate) tetrahydrate and a discussion of the ammonium ion. *Acta Crystallographica*, **B28**, 683–693.

Krivovichev S.V. (2013) Structural complexity of minerals: Information storage and processing in the mineral world. *Mineralogical Magazine*, **77**, 275–326.

Lussier A.J., Burns P.C. and King-Lopez R. (2016) A revised and expanded structure hierarchy of natural and synthetic hexavalent uranium compounds. *The Canadian Mineralogist*, **54**, 177–283.

Mandarino J.A. (1981) The Gladstone-Dale relationship – Part IV: The compatibility concept and its application. *The Canadian Mineralogist*, **19**, 441–450.

Plášil J., Kampf A.R., Kasatkin A. V., Marty J., Škoda R., Silva S. and Čejka J. (2013) Meisserite, $Na_5(UO_2)(SO_4)_3(SO_3OH)(H_2O)$, a new uranyl sulfate mineral from the Blue Lizard mine, San Juan County, Utah, USA. *Mineralogical Magazine*, **77**, 2975–2988.

Plášil J., Kampf A.R., Kasatkin A.V. and Marty J. (2014) Bluelizardite, $Na_7(UO_2)_3(SO_4)_4Cl(H_2O)_2$, a new uranyl sulfate mineral from the Blue Lizard mine, San Juan County, Utah, USA. *Journal of Geosciences*, **59**, 145–158.

Pouchou J.-L. and Pichoir F. (1991) Quantitative analysis of homogeneous or stratified microvolumes applying the model "PAP." Pp. 31–75 in: *Electron Probe Quantitation*. Springer US, Boston, MA.

Sheldrick G.M. (2015a) *SHELXT* – Integrated space-group and crystal-structure determination. *Acta Crystallographica*, **A71**, 3–8.

Sheldrick G.M. (2015b) Crystal structure refinement with *SHELXL*. *Acta Crystallographica*, **C71**, 3–8.

Tyumentseva S.O., Kornyakov V.I., Britvin N.S., Zolotarev A.A. and Gurzhiy V.V. (2019) Crystallographic insights into uranyl sulfate minerals formation: Synthesis and crystal structures of three novel cesium uranyl sulfates. *Crystals*, **9**, 660.